AtomicJ: An open source software for analysis of force curves

Paweł Hermanowicz,[1,a)] Michał Sarna,[2] Kvetoslava Burda,[2] and Halina Gabryś[1]
[1]*Department of Plant Biotechnology, Faculty of Biochemistry, Biophysics and Biotechnology, Jagiellonian University, Gronostajowa 7, 30–387 Kraków, Poland*
[2]*Department of Medical Physics and Biophysics, Faculty of Physics and Applied Computer Science, AGH University of Science and Technology, al. Mickiewicza 30, 30-059 Kraków, Poland*

(Received 24 February 2014; accepted 23 May 2014; published online 18 June 2014)

We present an open source Java application for analysis of force curves and images recorded with the Atomic Force Microscope. AtomicJ supports a wide range of contact mechanics models and implements procedures that reduce the influence of deviations from the contact model. It generates maps of mechanical properties, including maps of Young's modulus, adhesion force, and sample height. It can also calculate stacks, which reveal how sample's response to deformation changes with indentation depth. AtomicJ analyzes force curves concurrently on multiple threads, which allows for high speed of analysis. It runs on all popular operating systems, including Windows, Linux, and Macintosh. © *2014 AIP Publishing LLC*. [http://dx.doi.org/10.1063/1.4881683]

I. INTRODUCTION

Analysis of force curves recorded with the Atomic Force Microscope (AFM) is a standard method of investigating mechanical properties at the nanoscale, especially suitable for biological samples. Mechanical properties of cells and tissues are often altered by diseases and their measurements have potential medical applications. For example, malignant cancer cells are usually more compliant than their normal or benign counterparts,[1,2] while increase in Young's modulus has been observed in glaucoma[3] and sickle cell disease.[4]

Estimation of mechanical properties based on force curves requires prior assumption of the contact mechanics model. The accuracy of results is often limited due to a mismatch between the model and the experiment. The actual shape of the AFM tip often does not match the shape assumed in the model, for example, when the rounded apex of the tip is not taken into account.[5] The material itself may not satisfy the assumptions of the model, especially at very small or large indentation depths.[6] The geometry of the sample also affects the results, for example, thin samples appear stiffer because of the rigid substrate.[7,8]

The freely available applications for analysis of AFM measurements do not fully address these issues. The most popular ones, WSXM[9] and Gwyddion,[10] are focused on image analysis, while OpenFovea,[11] an application for analysis of force curves, supports only basic contact models. To fill this gap, we built AtomicJ, an open source Java application. The main goals of our application are to allow for both fast and reliable analysis of large sets of force curves and to provide tools for analysis and three-dimensional visualization of force maps.

AtomicJ calculates Young's modulus, adhesion force, sample height, and transition indentation. It can generate both two-dimensional maps of the mechanical properties and three-dimensional stacks, series of frames that show the spatial distribution of a particular quantity calculated for a certain force or indentation depth. It can use AFM images in the analysis of force maps, for example, to automatically find sample thickness or to partition a force map into multiple batches of curves. AtomicJ implements a wide range of contact models, among them models for thin[12,13] and hyperelastic[14–16] samples, for blunt tips,[5,17] the exact model for the sphere,[18] and models of adhesive contact.[19–22] We also implemented new procedures for identification of the contact point and identification of model deviations, which reduce effects of deviations at large indentation depths. Some of the implemented models are more computationally demanding than the simpler, commonly used ones. To ensure high performance, AtomicJ processes force curves concurrently on multiple threads.

AtomicJ is an open source software, so researchers can adapt it to implement their own solutions. Analysis of force curves is influenced by the choice of specific procedures, for example, the procedure used for identification of the contact point.[23] Use of open source code can improve the reproducibility of analysis and make it easier to compare results obtained by different groups.

II. PROCESSING OF FORCE CURVES

Processing of force curves is performed in two stages. First, the point of the initial contact between the tip and the sample is found and the force-indentation data are extracted from the force curve. The appropriate contact model is then fitted to the force-indentation data and Young's modulus is calculated from the fit.

A. Identification of the contact point

Accurate identification of the contact point is crucial for reliable estimation of Young's modulus.[23] AtomicJ supports both manual and automatic identification of the contact point.

The classical automatic procedure finds the contact point through successive search. Every point of the curve is assumed a trial contact point, a polynomial is fitted to the pre-contact part, and the appropriate contact model is fitted to the force-indentation data. The corresponding sums of squares

a)Author to whom correspondence should be addressed. Electronic mail: pawel.hermanowicz@uj.edu.pl.

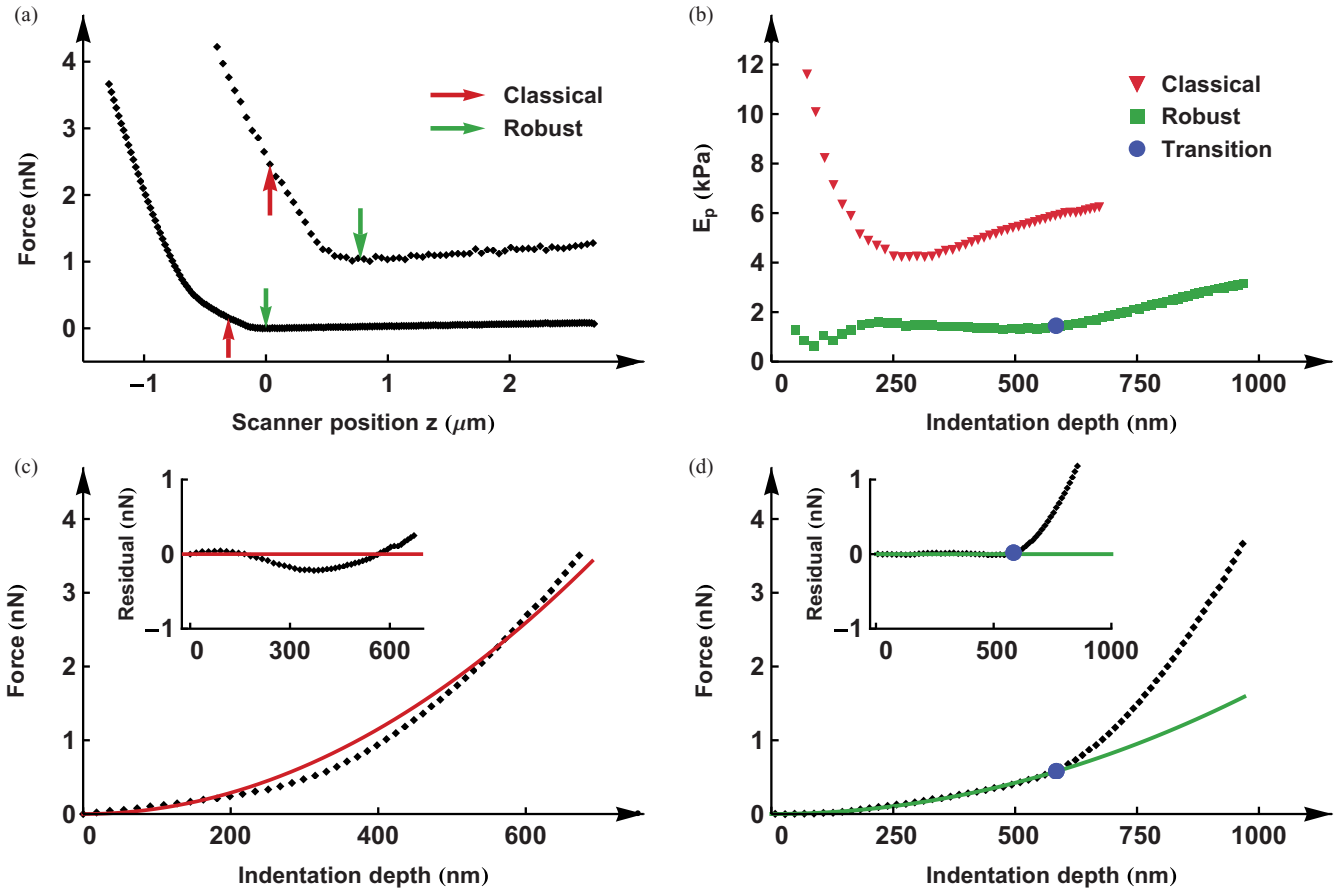

FIG. 1. Behavior of the robust and classical contact identification procedures in the presence of deviations from the model. (a) The Sneddon's model for the cone was used to analyze a typical force curve collected on a human cancer prostate cell. The contact points identified with the robust and classical procedure are marked with arrows. A close-up of the vicinity of the contact point is shown in the inset. (b) Pointwise Young's modulus E_p as a function of indentation depth, calculated based on the contact point obtained with the robust and the classical procedure. (c)–(d) The force–indentation curves obtained with (c) the classical (OLS fit shown) and (d) the robust procedure (HLTS fit). The residual plots are shown in insets. Note that the contact point obtained with the classical procedure is inaccurate, even though it provides better fit. Every fifth point is plotted in all curves.

are recorded. The point which gives the lowest total sum of squares is accepted as the contact point.[12] The total sum of squares is usually a unimodal function of the contact point position, so faster golden section search can be used instead of full successive search.[24]

The classical procedure is accurate for well-behaved curves, but when gross deviations from the model are present the true contact point leads to a suboptimal fit and is missed by the procedure (Figs. 1(a) and 1(c)). For analysis of curves that exhibit deviations from the model at large indentation depths, we designed a robust successive search method. The proposed procedure consists of three steps:

1. The precontact part of the curve is first roughly identified with the classical procedure and then fitted with a polynomial using the robust high coverage method,[25] which fits the bulk of data even if outliers are present.
2. The low force points, i.e., points deviating from the precontact fit less than m times the median of absolute values of residuals, are found. The parameter m controls the tradeoff between resistance to deviations and efficiency of dealing with random noise. It must be large enough to ensure that the contact point is among the low force points.
3. Every low force point is assumed a trial contact point. A polynomial is fitted to the precontact part with least squares and the contact model is fitted to the force-indentation data, using the least trimmed sum of squares (LTS),[26] with additional requirement that all the low force points are given non-zero weights. The point which gives the lowest total sum of squares is accepted as the contact point.

We tested the resistance of the classical and robust procedures to model deviations on force curves collected on human prostate cancer cells, which exhibit stiffening at large indentation depths (Fig. 1). The values of Young's modulus estimated with the robust procedure (Fig. 2(a)) are smaller than those estimated with the classical procedure (Fig. 2(b)) and their distribution is closer to the normal distribution.

B. Supported contact models

The contact model used for analysis of force curves should be appropriate for the shape of the tip and the properties of the sample. AtomicJ supports several models,[27] among them models for a linear elastic sample deformed with a cone[28] and pyramid[29] that are commonly used for curves

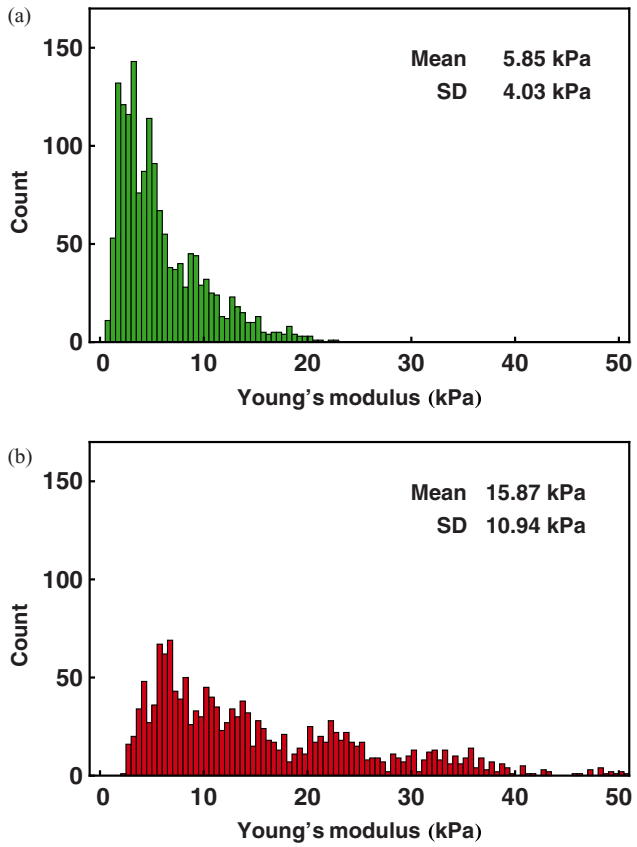

FIG. 2. Young's modulus of prostate cancer cells calculated with classical and robust approaches. Histograms show values calculated for prostate cancer cells. The robust procedure for contact point identification and HLTS method for fitting the contact model were used in (a), while the classical procedure for contact point identification and least squares fits were used in (b). Ten force curves were collected at each of 157 sites, located on ten different cells.

collected with regular AFM tips. These models are fast and easy to fit, but the results may not be accurate, as they do not take into account the round apex of the tip. For more accurate analysis, we implemented models for blunt cone,[5] blunt pyramid,[17] and models of adhesive[22] and noadhesive[30] hyperboloidal contact.

We implemented several models of spherical contact, used for curves collected with colloidal probes. The Hertz's model for sphere is suitable for nonadhesive contact, DMT[19] model for adhesive contact with stiff samples, and JKR[20] model for adhesive contact with compliant samples, including biological samples. Those models are frequently used, although their accuracy may be limited when indentations are deep.[21] They employ the parabolic approximation for the profile of sphere, which require that the contact radius is much smaller than the sphere radius. For analysis of deep indentations with colloidal probes we implemented the exact Sneddon's model for the sphere[18] and the Maugis' model of adhesive contact.[21]

Most models assume that sample thickness is multiple times greater than the indentation depth. If the sample is thin, the rigid substrate contributes to the force acting on the tip,[7] which leads to overestimation of Young's modulus. AtomicJ implements the corrections for the effect of substrate, derived for the sphere[12] and for the cone.[13] When these corrections are applied to force maps, AtomicJ can use the topography image to calculate sample thickness in the positions where curves were collected. It can also apply different forms of the corrections to different regions of the sample, selected on the image. The corrections depend on sample's adherence, which may vary in different locations, especially for cells.[13]

Nonlinear elastic behavior may also affect the calculated values of Young's modulus. Strain stiffening has been observed for numerous biological materials and is regarded as an adaptation preventing tissue damage.[33,34] Analysis of large strain behavior can be performed with hyperelastic models. For spherical contact, AtomicJ supports Fung's[14,16] and Ogden's[15,16] models, which describe well the nonlinear behavior of various biological tissues.

Contact models can be fitted to force-indentation data with a classical or robust regression method. The choice of the method should be based on the scale of deviations from the model. The most resistant to deviations are robust methods – four are available for the AtomicJ users: LTS,[26] LTA,[31,32] and their two-stage modifications HTLS (fit in Fig. 1(d)) and HLTA.[25] They provide accurate fits as long as more than half of the data points follow the model. AtomicJ estimates the depth of indentation at which the force-indentation curve starts to deviate from the contact model and reports it as the *transition indentation* (Figs. 1(b) and 1(d)). Transition indentation coincides with the onset of sample stiffening at large indentation depths (Fig. 8). The procedure for estimation of transition indentation is based on the robust estimators with high coverage.[25] If the force-indentation data do not exhibit pronounced deviations from the model, the contact model can be fitted with standard least squares or least absolute deviations procedures, which better deal with random noise. The maximal indentation depth is then reported as the transition indentation.

Young's modulus can be also calculated separately for each indentation depth. The pointwise modulus curve can be used to study the mechanical properties of subcellular structures, for example, stress fibers.[35,36] AtomicJ plots the pointwise modulus curve for each force curve. For force maps, it generates a stack of frames that show the two-dimensional spatial distribution of pointwise modulus calculated for different indentation depths.

III. 3D VISUALIZATION OF FORCE MAPS

Force maps can reveal how sample's response to deformation changes with indentation depth. This can be presented in the form of stacks. Stacks consist of a series of frames that show the spatial distribution of some quantity, calculated for a particular force F, indentation depth δ, or tip displacement σ. Stacks can be cross-sectioned to show how the visualized quantity varies in the direction perpendicular to the sample surface. AtomicJ generates several types of stacks. To avoid confusion, we will use a simple notation to identify stack type: (q | t), where q is the quantity displayed in frames and t is the quantity that identifies the frames.

The first group of stacks generated by AtomicJ is based on force contours (Fig. 3). Force exerted on the sample can be treated as a function of the position in the x-y plane and either

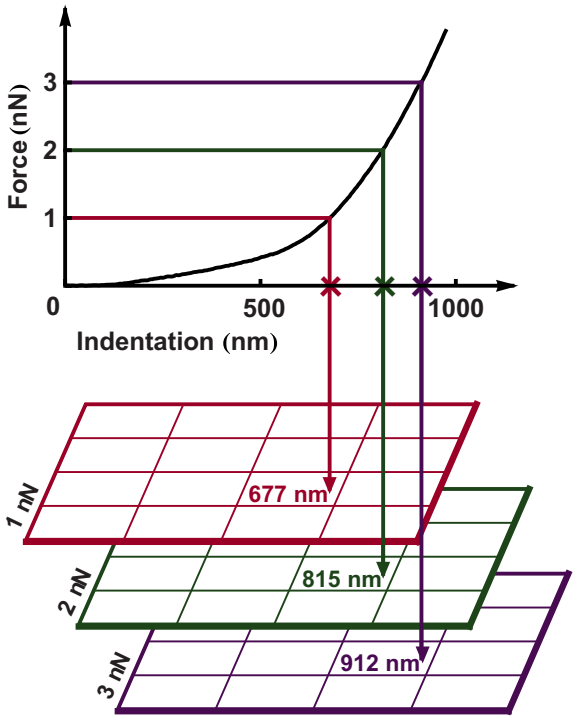

FIG. 3. Force contour stack. The indentation depth corresponding to a particular force is found for each curve and displayed in a two-dimensional array. Such arrays are calculated for multiple force values to create a stack.

the depth of indentation δ or tip displacement σ. Each frame of such a stack is a contour of this function for a particular value of force F, i.e., the set of all points (x, y, δ) or (x, y, σ) for which force equals F.

The force contour stack for tip displacement (σ | F) shows how sample topography is affected by increasing loading force, mimicking the topographic images obtained with increasing loads in the contact imaging mode. Similar stacks were first used to study human platelets.[37] The frame for zero force is the true topography of the sample, identical to the image formed by mapping the z-position of the contact point. Stiffer structures buried beneath the surface appear in the frames calculated for higher forces, and the sample itself appears lower due to compression. Both effects can be observed on human fibroblasts. The force of 3 nN compresses fibroblasts by 1 μm, bringing out stiffer fibers (Fig. 4, arrow) that are not visible in the frame for 0 nN.

The force contour stack for indentation depth (δ | F) shows how deeply the sample is deformed by loading forces. It is independent of sample topography, which makes it useful for visualization of sample compliance. The deformation produced by the force of 1 nN on a fibroblast is shown in Fig. 5(a). The cross section was cut along the white line with an arrowhead. We can clearly distinguish between more compliant cell body (left triangle) and the stiffer surroundings (right triangle). Overlaying the profile extracted from the contact point map shows the relationship between compliance and topography.

The second group of stacks consists of frames calculated for a particular indentation depth δ (Fig. 6(a)) or tip displacement σ (Fig. 6(b)), given by

$$\sigma = z_{top} - z_0 + \delta,$$

where z_{top} is the contact point at the highest point on the sample, z_0 is the contact point at the current location.

The pointwise modulus stack ($E_p(\delta)$ | δ) shows the spatial distribution of pointwise modulus, i.e., Young's modulus calculated for a particular indentation depth from single points on the force-indentation curve. In the cross section of a stack generated for a fibroblast (Fig. 5(b)), we observe how pointwise modulus varies with indentation depth. For small depths it is much greater than the bulk Young's modulus. This *small-depth stiffening* appears to be independent of the magnitude of the bulk Young's modulus, as it is visible both in the most

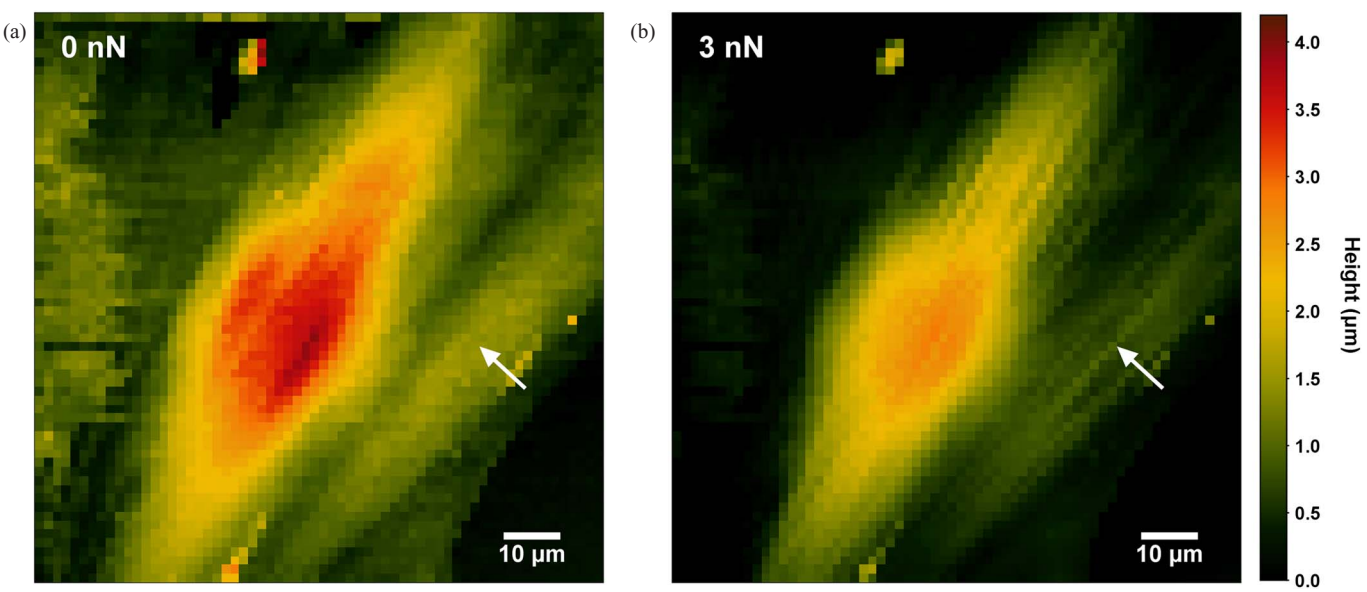

FIG. 4. Effect of loading force on sample topography. Frames from the force contour stack (σ | F), calculated for 0 nN (a) and 3 nN (b) show the topography of a fibroblast. The frame for 0 nN shows the true topography, while in the frame for 3 nN the topography is deformed by the loading force of 3 nN. Notice that due to unequal deformation of the sample, stiffer subcellular features become visible when loading is applied (fiber denoted by an arrow).

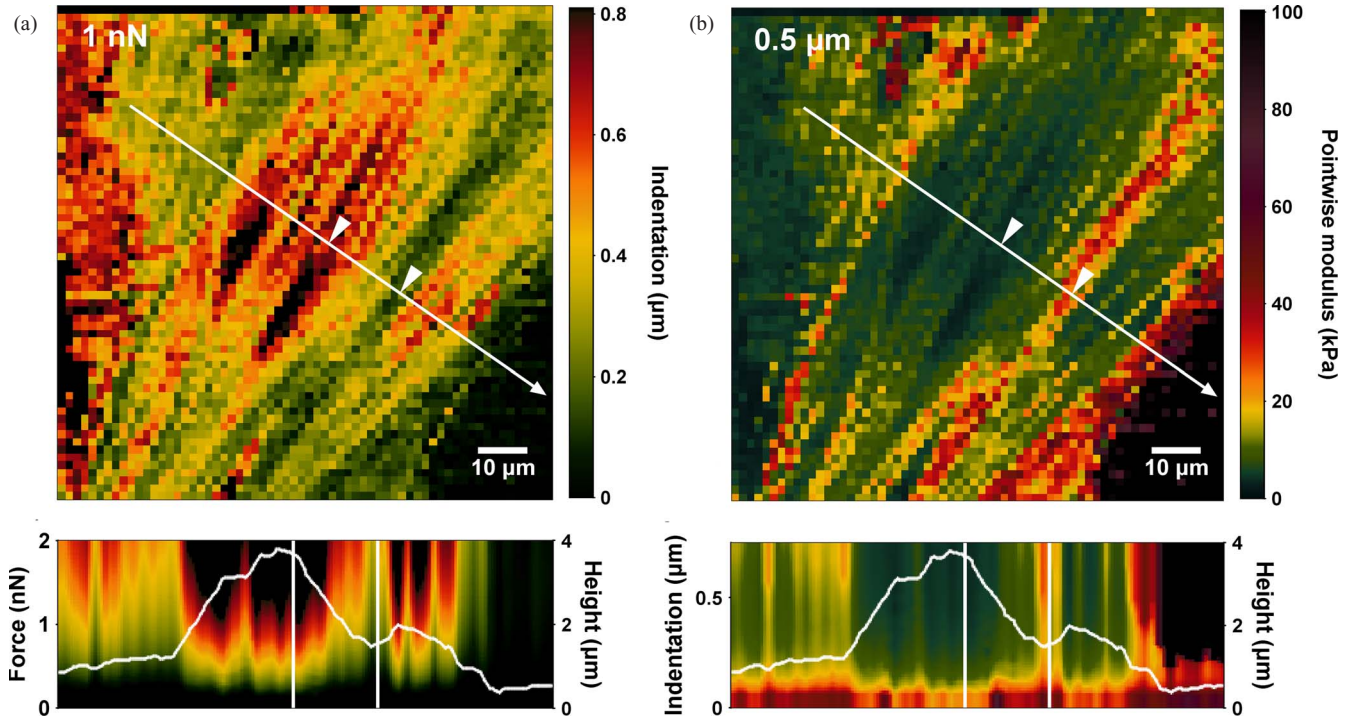

FIG. 5. Visualization of sample compliance with force stack and pointwise modulus stack. Frames from the force ($\delta \mid$ F) (a) and pointwise modulus stacks (E_p (δ) $\mid \delta$) (b) for a fibroblast. Both stacks were cross sectioned along the 100 μm long white lines. The position of the triangular markers corresponds to the position of white, vertical lines in the cross sections below. The cross sections are overlaid with height profile extracted from the contact point map. (a) The frame from force stack shows the differences in the depth of indentation produced by the force of 1 nN. We can distinguish between more compliant material in the highest, central part of the cell (left triangle), and stiffer surroundings (right triangle). (b) The pointwise modulus stack shows the pointwise Young's modulus, calculated for indentation depth of 0.5 μm. The more compliant central part of the cell has smaller pointwise modulus (left triangle).

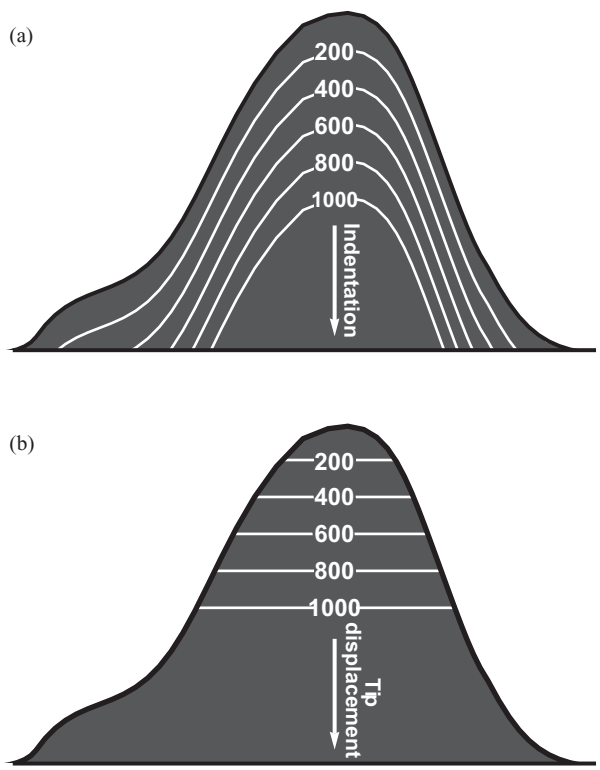

FIG. 6. Stacks for indentation depth δ and tip displacement σ. Stacks for indentation depth (a) are independent of topography, which makes them convenient tools to examine how depth-dependent properties vary in different parts of the sample. Stacks for tip displacement (b) conserve the sample topography and can be used to examine the relationship between topography and mechanical properties.

compliant and in the stiff parts of the cell. At medium indentation depths, pointwise modulus decreases. At large depths, it rises again in thin part of the cell, but stays more or less constant in the cell body.

The stacks with frames calculated for different values of tip displacement σ conserve sample topography. Frames resemble slices cut by planes parallel to the substrate. The shape of the sample is visible in the cross section and the relationship between topography and mechanical properties can be observed. For example, in the cross section of a pointwise modulus stack ($E_p \mid \sigma$) (Fig. 7) we can notice that the small-depth stiffening is independent of the sample topography, as it is visible both in the thin and the thick parts of the cell.

The stiffening stack (E_p (δ) $-$ E$\mid \delta$) is designed for visualization of the increase in sample's apparent stiffness at

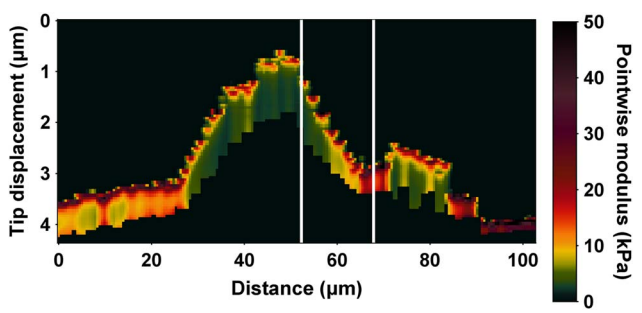

FIG. 7. Cross section of pointwise modulus stack (Ep (σ)$\mid \sigma$). The shape of the cell is visible in the cross section, made along the same line as in Fig. 5. Notice the large changes in pointwise modulus both along the section line, and with indentation depth.

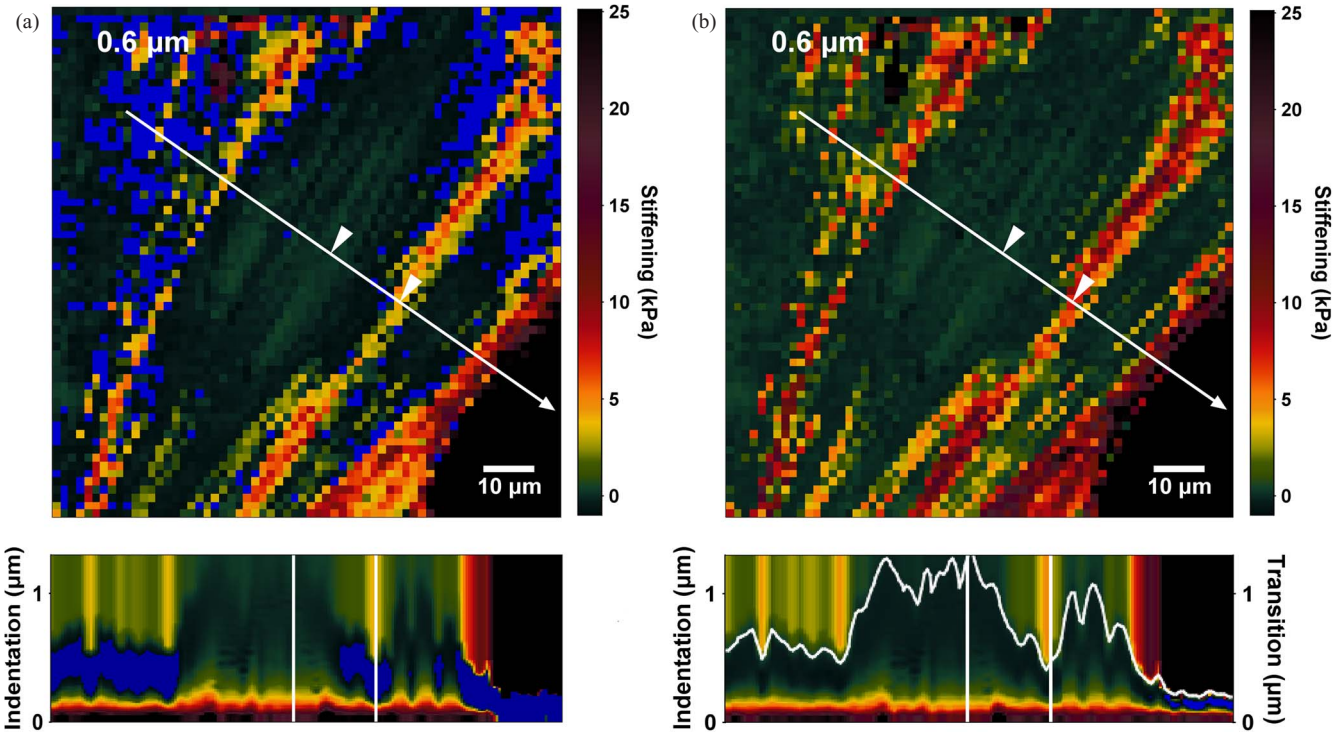

FIG. 8. Stiffening stack (Ep (δ) − E| δ). The stiffening stack shows the difference between pointwise modulus for a particular indentation depth (frames for 0.6 μm are visible) and Young's modulus from the model fit. The fit can be obtained using least squares (a) or robust HLTS estimator (b). The choice of regression estimator influences the quality of the stack. When least squares are used, stiffening is negative for medium depths (values below −1 kPa are in blue). This artifact is caused by overestimation of Young's modulus by least squares. Transition indentation profile is overlaid on the stack cross section in (b). Note that it coincides with the onset of sample stiffening.

large indentation depths. Increase in stiffness with depth may be caused by nonlinear elasticity of the material itself, or by the presence of stiffer structures within the sample.[35] Stiffening is the difference between the pointwise modulus for a particular depth and the Young's modulus calculated from the model fit, which ideally should be close to the true Young's defined for the linear elastic range. The model can be fitted using least squares (Fig. 8(a)) or robust estimators (Fig. 8(b)). Stiffening calculated relative to Young's modulus from least squares fits is often negative for medium indentation depths, as if the sample became more compliant (values below −1 kPa are blue in Fig. 8(a)). The reason is that the least squares fits are affected by stiffening at larger indentation depths and overestimate Young's modulus. This artifact is absent when the robust estimator is used (Fig. 8(b)). Transition indentation coincides with the onset of sample stiffening at large indentation depths. Its profile does not simply follow sample topography (compare the transition indentation profile in Fig. 8(b) and the topography profile in Fig. 5), but rather reflects the presence of stiffer, subcellular structures.

IV. USER INTERFACE AND WORKFLOW

AtomicJ is equipped with a graphical user interface (GUI), consisting of the main window, a number of dialogs for displaying results, and assistants which help users to accomplish complex tasks. The AtomicJ User's Manual[38] contains detailed guidelines on how to use its interface.

A. Force curve processing

Force curves and force maps are processed using a dedicated assistant. The processing assistant (Fig. 9(a)) gathers the necessary settings in multiple steps and ensures that they are specified in the right order. Force curves are loaded in batches. A batch may contain both force curves and force maps, and a single force map can be split into multiple batches, corresponding to different regions selected on an AFM image. The processing settings are specified for each batch independently. This provides the flexibility necessary for simultaneous processing of curves recorded in different AFM experiments. To speed up the procedure, the settings can be exported to a text file and later reused.

Processing can be manual or automatic. In the manual mode the user picks the contact point on the curve with the mouse. The user can drag the contact point manually and observe the changes in Young's modulus and the model fit. One or two coordinates of the point identified for one curve can be used in the analysis of the remaining curves, which may be useful for fast, cursory analysis of multiple curves recorded at the same location. In the automatic mode no input is required from the user, apart from selecting the procedure for contact point identification and the regression method for fitting the contact model. AtomicJ leaves this choice entirely to the user. For example, a robust method can be used for model fits along with the classical procedure for contact point identification, or different combinations can be used for different batches.

The quantitative results of processing include Young's modulus, coordinates of the contact and transition points,

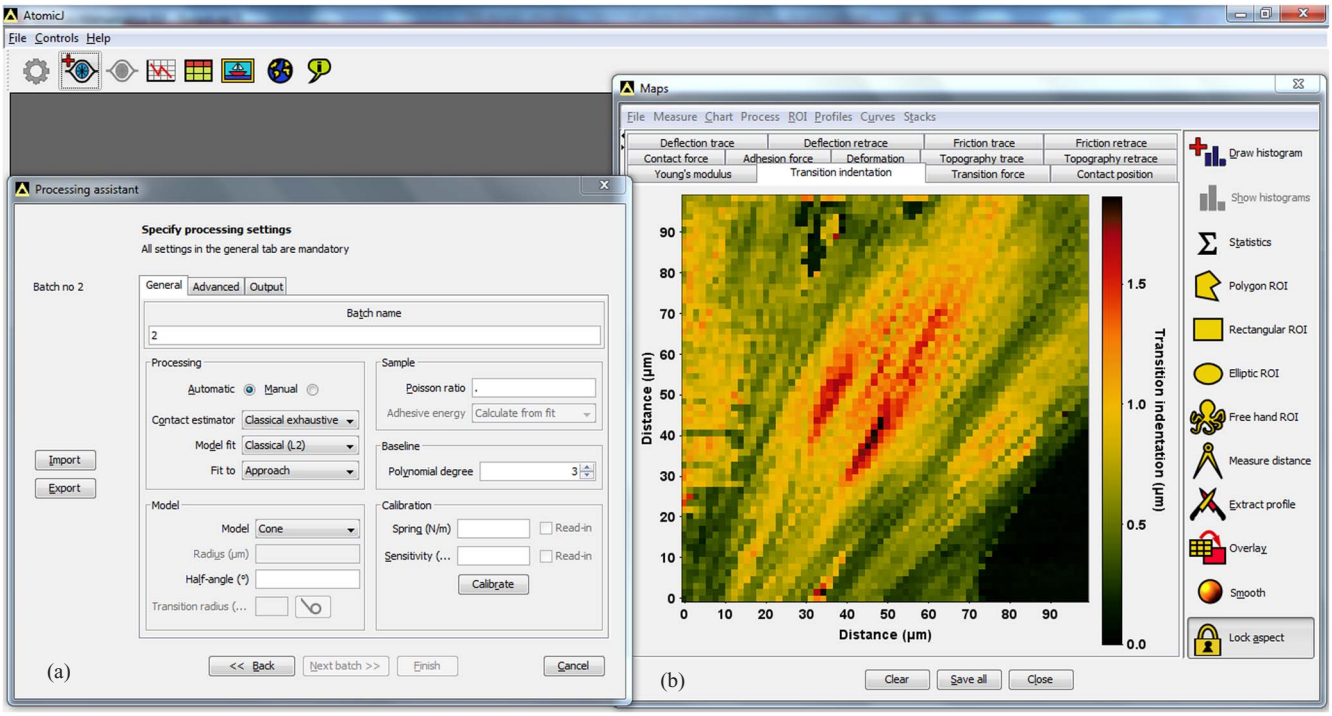

FIG. 9. Screenshot of AtomicJ GUI. (a) The processing assistant is used for selection of the force curves and maps that are to be analyzed and for specifying how the analysis should be performed. (b) The map dialog displays the maps of mechanical properties. The map of transition indentation is visible.

adhesion force and deformation. Force curves, force-indentation curves, and pointwise Young's modulus curves are plotted. The results can be analyzed statistically, visualized as histograms or box-plots, saved to a file or copied to a spreadsheet application. If the results of processing are unsatisfactory, selected force curves can be recalculated with different settings.

B. Maps and images

The results of processing of force maps are displayed as maps of mechanical properties (Fig. 9(b)). AtomicJ offers several tools for processing and analysis of maps, among them procedures for noise removal, background correction, edge detection, and convolution with arbitrary kernels. Processing of maps is facilitated by regions of interest (ROIs). ROIs can be rectangular, elliptical, polygonal, or of arbitrary shape and can be easily moved and reshaped. They can be used to restrict the range of image processing operations, to calculate statistics and histograms for parts of the sample, or to measure area and shape factors of objects in the map. The maps are linked to the underlying grid of force curves. The user may inspect or recalculate the force curves for a particular position in the map or the selected ROIs.

Histograms, box plots, and statistics can be calculated for whole maps or the individual ROIs. If an image of the sample is available, statistics and histograms are calculated within the same region both for the maps and for the image, which helps to understand the correlation between mechanical properties and the image. Height profiles can be extracted from maps using nearest neighbor, bilinear, or bicubic spline interpolation. They are instantly updated when the profile lines are dragged around the map or the map itself is modified.

Although AtomicJ is designed primarily for extracting mechanical properties from force curves, it can process images as well. The same tools are available for maps and images.

C. Stacks

Stacks can be created for a whole force map, or for the selected ROIs. They are displayed in a separate dialog, where the stack can be played as a movie. Several tools can be accessed from the stack dialog. Statistics and histograms can be calculated for single frames, while the differences between frames can be inspected using live histograms, which are instantly updated when the stack is played. Stacks support regions of interest, as well as area and distance measurements.

Changes of the visualized quantity across the depth of the sample can be analyzed with cross sections. AtomicJ can extract cross sections along arbitrary lines, selected by the user with the mouse, which are updated when the user moves the section lines. Stack cross section can be overlaid with map profiles to reveal the correlations with the quantities displayed in the 2D maps, for example, sample topography. In addition, the user may inspect the force curve and the calculated quantities for a particular position in the stack or its cross section.

D. File formats

AtomicJ can read files with images and force curves collected by microscopes from Agilent Technologies, JPK

Instruments, and Bruker. It can also read plain text files. AtomicJ supports a wide range of output formats. Maps can be saved in a vector format (EPS, PS, SVG, and PDF), a raster format (PNG, TIFF, JPEG, JPEG2000, GIF, EMF, BMP, and Portable Pixmap), or as plain text file (CSV or TSV). Stacks can be saved as AVI movies or multipage TIFFs. Individual frames can be saved separately. AtomicJ supports multithreaded batch saving of multiple charts.

V. DEPENDENCIES AND AVAILABILITY

AtomicJ is written in Java SE 7 and uses only open-source libraries. JFreeChart is used for chart plotting, JAMA is used for matrix manipulations, and Commons Math is used as a general-purpose mathematical library, FreeHEP, Sanselan, Commons Compress, Bio-Formats,[39] and iText® 2.1.5 provide support for output file formats.

AtomicJ is licensed under the terms of the GNU General Public License and can be downloaded from SourceForge http://sourceforge.net/projects/jrobust, together with the manual and short movies showing how to use it. It is available in two distributions: the distribution for 64-bit Windows, bundled with Java 7 Runtime Environment, and the platform-independent distribution, that runs on all popular operation systems, among them Windows, Linux, and Mackintosh.

VI. EXPERIMENTS

Force curves were collected using an Agilent 5500 Atomic Force Microscope (Agilent Technologies), with silicon nitride cantilevers (Veeco Probes (nominal tip radius of 20 nm, half-angle 25°, nominal spring constant 0.01 N m^{-1}). The spring constant used for calculation of Young's modulus was determined using the thermal tune method. Measurements were performed in culture medium at 37 °C.

Human prostate carcinoma DU-145 cells were cultivated in DMEM-F12 HAM (Sigma), supplemented with 10% fetal bovine serum and antibiotics, and maintained at 37 °C in a 5% CO_2 humidified atmosphere. The curves used for assessment of the contact estimators were collected on the prostate cancer cells at the rate of 1 Hz and with deep (>500 nm) indentations, to obtain pronounced deviations from the contact models. We analyzed them using either the classical successive search procedure for contact point identification and least squares for contact model fits, or with the robust procedure, with the HLTS fits. They are included in AtomicJ test files.

The stacks were generated from 64 × 64 force maps collected on human fibroblasts. Because the indentations were shallow, we processed force maps with the classical contact point estimator, combined with robust HLTS method for model fits. The force map used in Figs. 4, 5, 7, and 8, together with the AFM image recorded within the same area, can be downloaded from http://sourceforge.net/projects/jrobust/.

ACKNOWLEDGMENTS

The authors would like to thank Dr. Marta Michalik for the fibroblast cells. This study was supported in part by the Polish Ministry of Science and Higher Education (PB 1395/B/P01/2007/33). The Faculty of Biochemistry, Biophysics, and Biotechnology of the Jagiellonian University is a beneficiary of European Union structural funds (Grant No. POIG.02.01.00-12-064/08, "Molecular biotechnology for health").

[1] M. Lekka, P. Laidler, D. Gil, J. Lekki, Z. Stachura, and A. Z. Hrynkiewicz, Eur. Biophys. J. **28**, 312 (1999).
[2] Q. S. Li, G. Y. H. Lee, C. N. Ong, and C. T. Lim, Biochem. Biophys. Res. Commun. **374**, 609 (2008).
[3] J. A. Last, T. Pan, Y. Ding, C. M. Reilly, K. Keller, T. S. Acott, M. P. Fautsch, C. J. Murphy, and P. Russell, Invest. Ophthalmol. Vis. **52**, 2147 (2011).
[4] J. L. Maciaszek and G. Lykotrafitis, J. Biomech. **44**, 657 (2011).
[5] D. J. Briscoe, K. S. Sebastian and M. J. Adams, J. Phys. D **27**, 1156 (1994).
[6] I. Sokolov, M. E. Dokukin, and N. V. Guz, Methods **60**, 202 (2013).
[7] C. Rotsch, K. Jacobson, and M. Radmacher, Proc. Natl. Acad. Sci. U.S.A. **96**, 921 (1999).
[8] J. Domke and M. Radmacher, Langmuir **14**, 3320 (1998).
[9] I. Horcas, R. Fernandez, J. M. Gomez-Rodriguez, J. Colchero, J. Gomez-Herrero, and A. M. Baro, Rev. Sci. Instrum. **78**, 013705 (2007).
[10] D. Nečas and P. Klapetek, Cent. Eur. J. Phys. **10**, 181 (2012).
[11] C. Roduit, B. Saha, L. Alonso-Sarduy, A. Volterra, G. Dietler, and S. Kasas, Nat. Methods **9**, 774 (2012).
[12] E. K. Dimitriadis, F. Horkay, J. Maresca, B. Kachar, and R. S. Chadwick, Biophys. J. **82**, 2798 (2002).
[13] N. Gavara and R. S. Chadwick, Nat. Nanotechnol. **7**, 733 (2012).
[14] Y. C. Fung, K. Fronek, and P. Patitucci, Am. J. Physiol. Heart. Circ. Physiol. **237**, H620 (1979).
[15] R. W. Ogden, Proc. R. Soc. London, Ser. A **326**, 565 (1972).
[16] D. C. Lin, D. I. Schreiber, E. K. Dimitriadis, and F. Horkay, Biomech. Model. Mechanobiol. **8**, 345 (2009).
[17] F. Rico, P. Roca-Cusachs, N. Gavara, R. Farre, M. Rotger, and D. Navajas, Phys. Rev. E **72**, 021914 (2005).
[18] I. N. Sneddon, Int. J. Eng. Sci. **3**, 47 (1965).
[19] B. V. Derjaquin, V. M. Muller, and Y. P. Toporov, J. Colloid. Interface Sci. **53**, 314 (1975).
[20] K. L. Johnson, K. Kendall, and A. D. Roberts, Proc. R. Soc. London, Ser. A **324**, 301 (1971).
[21] D. Maugis, Langmuir **11**, 679 (1995).
[22] Y. Sun, B. Akhremitchev, and G. Walker, Langmuir **20**, 5837 (2004).
[23] S. L. Crick and F. C.-P. Yin, Biomech. Model. Mechan. **6**, 199 (2007).
[24] D. C. Lin, E. K. Dimitriadis, and F. Horkay, J. Biomech. Eng. **129**, 430 (2007).
[25] D. J. Olive and D. M. Hawkins, Stat. Prob. Lett. **63**, 259 (2003).
[26] R. J. Rousseeuw and A. M. Leroy, *Robust Regression and Outlier Detection* (Wiley, New York, 1987).
[27] See supplemental material at http://dx.doi.org/10.1063/1.4881683 for the force-indentation relations of the supported contact models.
[28] J. W. Harding and I. N. Sneddon, Proc. Camb. Philos. Soc. **41**, 16 (1945).
[29] G. Bilodeau, ASME J. Appl. Mech. **59**, 519 (1992).
[30] B. B. Akhremitchev and G. C. Walker, Langmuir **15**, 5630 (1999).
[31] G. Bassett, Am. Stat. **45**, 135 (1999).
[32] D. M. Hawkins and D. Olive, Comput. Stat. Data Anal. **32**, 119 (1999).
[33] C. Storm, J. J. Pastore, F. C. MacKintosh, T. C. Lubensky, and P. A. Janmey, Nature (London) **435**, 191 (2005).
[34] Y. C. Lin, N. Y. Yao, C. P. Broedersz, H. Herrmann, F. C. MacKintosh, and D. A. Weitz, Phys. Rev. Lett. **104**, 058101 (2010).
[35] K. D. Costa, A. J. Sim, and F. C-P. Yin, J. Biomech. Eng. **128**, 176 (2006).
[36] L. Lu, S. J. Oswald, H. Ngu, and F. C.-P. Yin, Biophys. J. **95**, 6060 (2008).
[37] M. Radmacher, M. Fritz, C. M. Kacher, J. P. Cleveland, and P. K. Hansma, Biophys. J. **70**, 556 (1996).
[38] AtomicJ User's Manual can be downloaded from its SourceForge page https://sourceforge.net/projects/jrobust/files/1.4/AtomicJ_Users_Manual.pdf.
[39] M. Linkert, C. T. Rueden, C. Allan, J.-M. Burel, W. Moore, A. Patterson, B. Loranger, J. Moore, C. Neves, D. MacDonald, A. Tarkowska, C. Sticco, E. Hill, M. Rossner, K. W. Eliceiri, and J. R. Swedlow, J. Cell Biol. **189**, 777 (2010).